Catalysis Today 242 (2015) 294–299

Contents lists available at ScienceDirect

Catalysis Today

journal homepage: www.elsevier.com/locate/cattod

# Ordered mesoporous and bulk $Co_3O_4$ supported Pd catalysts for catalytic oxidation of o-xylene

Yafei Wang [a], Changbin Zhang [a], Yunbo Yu [a], Renliang Yue [b], Hong He [a,*]

[a] Research Center for Eco-Environmental Sciences, Chinese Academy of Sciences, Beijing 100085, PR China
[b] Institute of Process Engineering, Chinese Academy of Sciences, Beijing 100190, PR China

ARTICLE INFO

*Article history:*
Received 14 April 2014
Received in revised form 17 June 2014
Accepted 24 June 2014
Available online 25 July 2014

*Keywords:*
Ordered mesoporous
Cobalt oxide
Palladium
Catalytic oxidation
o-Xylene

ABSTRACT

Ordered mesoporous $Co_3O_4$ (3D) and the bulk counterpart $Co_3O_4$ (B) were prepared by a nanocasting route and precipitation method, respectively. Pd was next loaded on both of them by an impregnation method. All catalysts were tested for the total oxidation of o-xylene in the temperature range of 150–300 °C. Mesoporous $Co_3O_4$ (3D) exhibited better activity than $Co_3O_4$ (B), and Pd addition further improved the catalytic activity of both the mesoporous and bulk $Co_3O_4$. The BET and TEM results indicated that the mesoporous catalysts had uniform channel dimensions and the mesostructure was little affected by Pd addition. The TPR and XPS data indicated that Pd was much more exposed on the surface of $Co_3O_4$ (3D) than that of $Co_3O_4$ (B). TPD results showed that Pd/$Co_3O_4$ (3DL) could activate the oxygen species more easily than Pd/$Co_3O_4$ (BL). Therefore, Pd/$Co_3O_4$ (3DL) presented the best activity among the four catalysts and achieved 90% conversion of 150 ppm o-xylene at 249 °C at a space velocity of 60,000 mL $g^{-1}$ $h^{-1}$.



## 1. Introduction

Volatile organic compounds (VOCs) are harmful to human health and the environment. Benzene, toluene and xylene (BTX) emitted from various industrial processes and transportation activities are among the major VOCs in air at large scale [1]. Many techniques have been developed for the abatement of BTX emission [2,3], such as adsorption, thermal oxidation, photocatalytic oxidation and catalytic oxidation. Catalytic oxidation is considered to be the most suitable pathway for the removal of VOCs owing to its easy application, high efficiency and low production of thermal $NO_x$ [4].

Over the last several years, the complete catalytic oxidation of BTX has been widely studied over supported noble metal and metal oxide catalysts. Supported noble metal catalysts such as those containing palladium, platinum, rhodium, silver and gold are regarded as promising catalysts for the oxidation of BTX. Among them, Pd-based catalysts are the most widely investigated catalysts due to their low cost and high catalytic activity for BTX oxidation in the low temperature range. Liotta [5] synthesized several catalysts by supporting noble metals on $Al_2O_3$, and found that Pd/$Al_2O_3$ was the best catalyst for the catalytic oxidation of benzene. Kim and Shim [6], and Centi [7] showed that Pd-based catalysts showed superior performance compared to other noble metals or mixed oxides for the oxidation of methane and BTX. The activity of Pd-based catalysts is greatly influenced by the characteristics of the support [7], such as porosity and redox properties.

In recent years, ordered mesoporous transition metal oxides have received great attention owing to their uniform channel dimensions, open porous structure and multiple oxidation states [8–13]. Ordered mesoporous $Co_3O_4$ was fabricated by some groups using different silica templates, such as KIT-5, SBA-15, SBA-16, KIT-6, and forming different replica mesoporous structures ((2d-hexagonal *P6mm*) (bicontinuous cubic *Ia3d*) (*Im3n*)) [11,14–18]. It was shown that the three-dimensional cubic *Ia3d* mesoporous structure had a more open porous system than other mesostructures, facilitating the absorption and diffusion of the VOC molecules during the catalytic oxidation of short-chain VOCs [13,18,19]. Due to their unique physicochemical properties, ordered mesoporous transition metal oxides have been directly used as catalysts for the oxidation reaction and also used as the supports for noble metals [13].

As reported in our previous work, a series of Pd/$Co_3O_4$ catalysts were prepared, and the effect of the different Pd loading methods on three-dimensional ordered mesoporous $Co_3O_4$ ($Co_3O_4$ (3D)) for catalytic oxidation of o-xylene was discussed in detail [20]. In this work, in order to further confirm the advantage of

* Corresponding author. Tel.: +86 10 62849123; fax: +86 10 62849123.
*E-mail address:* honghe@rcees.ac.cn (H. He).

http://dx.doi.org/10.1016/j.cattod.2014.06.032
0920-5861/

3D structure for o-xylene oxidation, non-mesoporous $Co_3O_4$ (B) and mesoporous $Co_3O_4$ (3D) were used as supports for Pd addition (Namely, $Pd/Co_3O_4$ (3DL) and $Pd/Co_3O_4$ (BL)) and the effect of different structure of the catalysts were studied.

## 2. Materials and methods

### 2.1. Catalyst preparation

Mesoporous $Co_3O_4$ (3D) was prepared using 3D cubic KIT-6 as a hard template [20].

Bulk $Co_3O_4$ (B) was prepared by the precipitation method [21]. Typically, 17.46 g cobalt nitrate hexahydrate ($Co(NO_3)_2{\cdot}6H_2O$) was dissolved in 150 mL of distilled water. The aqueous solution of $Co(NO_3)_2$ was heated to 50 °C and poured into 150 mL of aqueous $Na_2CO_3$ solution kept at 50 °C, then stirred for 3 h. The precipitate was thoroughly washed with distilled water and filtered. The solid obtained was dried at 100 °C overnight and calcined in air at 300 °C for 3 h to transform it to $Co_3O_4$.

1%$Pd/Co_3O_4$ (BL) and 1%$Pd/Co_3O_4$ (3DL) were prepared by impregnation of $Co_3O_4$ (B) and $Co_3O_4$ (3D) using an aqueous solution of $Pd(NO_3)_2$ (palladium(II) nitrate hexahydrate, Aldrich). After stirring for 2 h, the excessive water was removed in a rotary evaporator at 60 °C. The samples were dried overnight at 110 °C and calcined at 500 °C for 3 h in air to decompose the metal salt adsorbed on the support.

### 2.2. Catalysts characterization

Power X-ray diffraction (XRD) was used to identify the crystalline phase present in the catalysts. A Bruker D8 Advance diffractometer with monochromatic Cu Kα source operated at 40 kV and 40 mA was used. TEM images were obtained using a JEOL JEM-2100 microscope, operating at 200 kV. $N_2$ adsorption–desorption isotherms were measured using a Quantachrome Quadrasorb IQ at liquid nitrogen temperature (77 K). The $H_2$ temperature programmed reduction ($H_2$-TPR) tests were carried out on a mass spectrometer (Hiden HPR20). Prior to each TPR run, the catalyst was pretreated in an air flow at 300 °C in a quartz reactor. After the reactor cooled to room temperature, Ar gas was fed into the reactor at 30 mL $min^{-1}$ for 30 min to purge any residual oxygen. The catalyst was then heated to 700 °C at a constant heating rate of 10 °C $min^{-1}$ under 5% $H_2$-Ar flow of 30 mL $min^{-1}$. The $O_2$-temperature-programmed desorption ($O_2$-TPD) tests were carried out on a Micromeritics Auto chem II 2920. The catalyst was pretreated in an oxygen flow at 300 °C in a quartz reactor. After the reactor was cooled to −50 °C, Ar gas was fed into the reactor at 50 mL $min^{-1}$ for 30 min to purge any residual oxygen. The catalyst was then heated to 700 °C at a constant heating rate of 10 °C $min^{-1}$ under 10% $H_2$-Ar flow of 50 mL $min^{-1}$. X-ray photoemission (XPS) measurements were recorded on a Scanning X-ray Microprobe (AXIS Ultra, Kratos Analytical, Inc.). Binding energy was calibrated with C 1s = 284.8 eV.

### 2.3. Catalytic activity tests

The catalytic activities of the catalysts were evaluated in a continuous flow fixed-bed quartz microreactor between 150 and 300 °C with 100 mg of catalyst (40–60 mesh). The reactant feed (flow rate = 100 mL/min) was composed of 150 ppm o-xylene and air, with the weight space velocity (WHSV) of 60,000 mL $g^{-1}$ $h^{-1}$. The outlet gas was analyzed online by a GC–MS (Agilent 6890-5973N, HP 5MS) and a GC (Shangfen GC-112A, TDX-01 column).

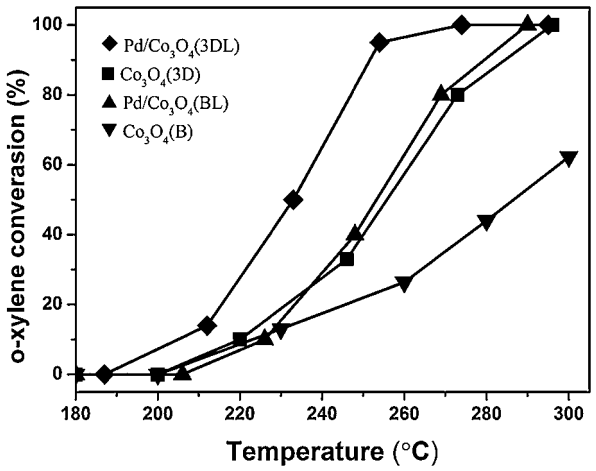


**Fig. 1.** o-Xylene conversion as a function of reaction temperature over the catalysts under the condition of o-xylene concentration = 150 ppm and WHSV = 60,000 mL $g^{-1}$ $h^{-1}$.

## 3. Results and discussion

### 3.1. Catalytic performance

According to Fig. 1, catalytic performance was in the order $Pd/Co_3O_4$ (3DL) > $Pd/Co_3O_4$ (BL) > $Co_3O_4$ (3D) > $Co_3O_4$ (B). The reaction temperatures $T_{50\%}$ and $T_{90\%}$ (corresponding to VOC conversion = 50% and 90%, respectively) were used to evaluate the catalytic performance, and the results are summarized in Table S1. It is seen that a $T_{90\%}$ value of 249 °C for o-xylene oxidation was achieved over $Pd/Co_3O_4$ (3DL), whereas the $T_{90\%}$ value was 277 °C for o-xylene oxidation over $Pd/Co_3O_4$ (BL). $CO_2$ and $H_2O$ were the only products and the carbon balance was around 99.5%, indicating that o-xylene can be completely oxidized on the catalyst. It is clear that mesoporous catalysts performed much better than bulk catalysts, suggesting that the structure is important for catalytic performance of the catalysts.

### 3.2. Structure analysis

#### 3.2.1. XRD

The low-angle XRD patterns of the $Co_3O_4$ (3D) and $Pd/Co_3O_4$ (3DL) catalysts are shown in Fig. 2(a). It can be seen that the hard template (KIT-6) exhibits the well-resolved diffraction peaks (2 1 1) and (3 3 2) and the shoulder peak (2 2 0), characteristic of a cubic *ia*3*d* mesostructure and indicating a high degree of ordering of this material [22]. The $Co_3O_4$ (3D) presented the (2 1 1) reflection at 2$\theta$ value of 1° with a peak intensity lower than that in the KIT-6 sample, suggesting that the mesostructure in the Co-containing catalysts was less ordered than their silica template. The Pd addition to $Co_3O_4$ resulted in a slight decrease of XRD peak intensity, but the mesoporous structure of $Pd/Co_3O_4$ (3DL) still remained, indicating that Pd addition had slight effect on the mesoporous $Co_3O_4$.

The large angle XRD patterns of the four catalysts are shown in Fig. 2(b). The materials exhibited peaks at 31.3°, 36.9°, 44.5°, 55.6°, 59.4°, and 65.3° (2$\theta$). All diffraction peaks could be assigned to the cobalt oxide according to JCPDS PDF 74-1657, indicating that the cobalt precursor was completely turned into crystalline cobalt oxide after calcination. No characteristic diffraction peaks of metallic Pd or oxidized Pd were observed in $Pd/Co_3O_4$ (3DL) and $Pd/Co_3O_4$ (BL), suggesting that Pd was well dispersed on the $Co_3O_4$.

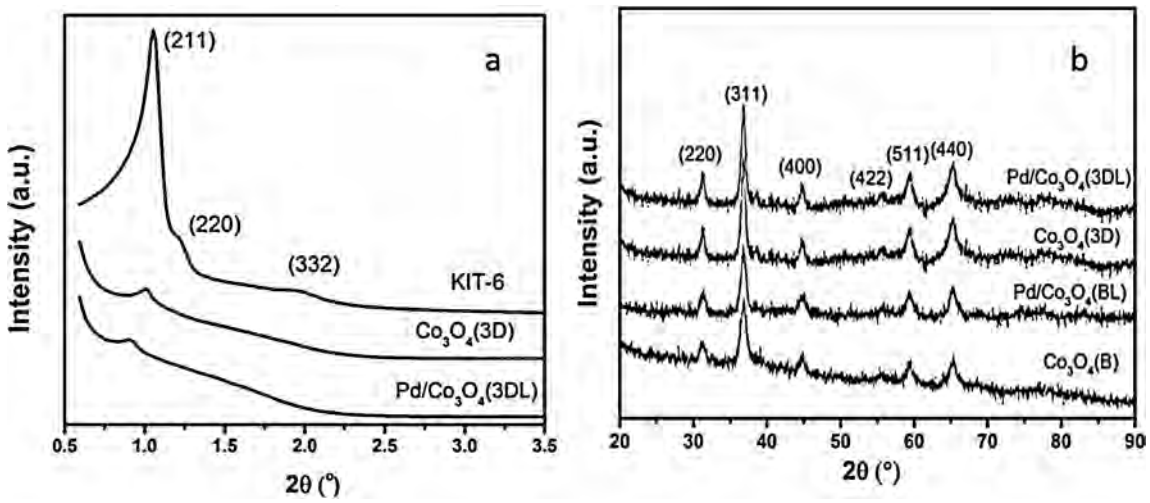


**Fig. 2.** Low-angle (a) and large-angle (b) XRD patterns of the $Pd/Co_3O_4$ catalysts.

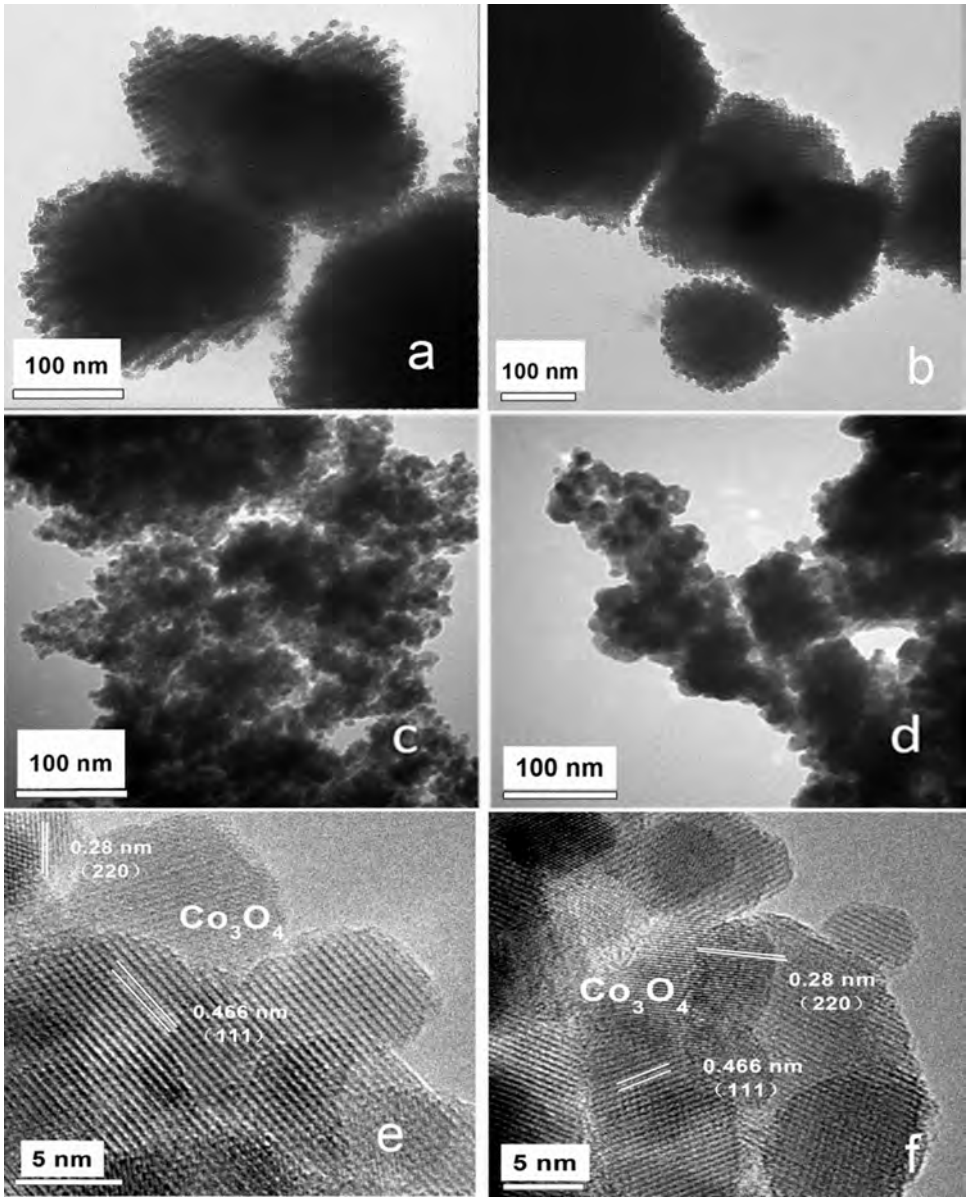


**Fig. 3.** TEM images of the catalysts: (a) $Co_3O_4$ (3D), (b) $Pd/Co_3O_4$ (3DL), (c) $Co_3O_4$ (B), (d) $Pd/Co_3O_4$ (BL); HRTEM images of (e) $Pd/Co_3O_4$ (3DL) and (f) $Pd/Co_3O_4$ (BL).

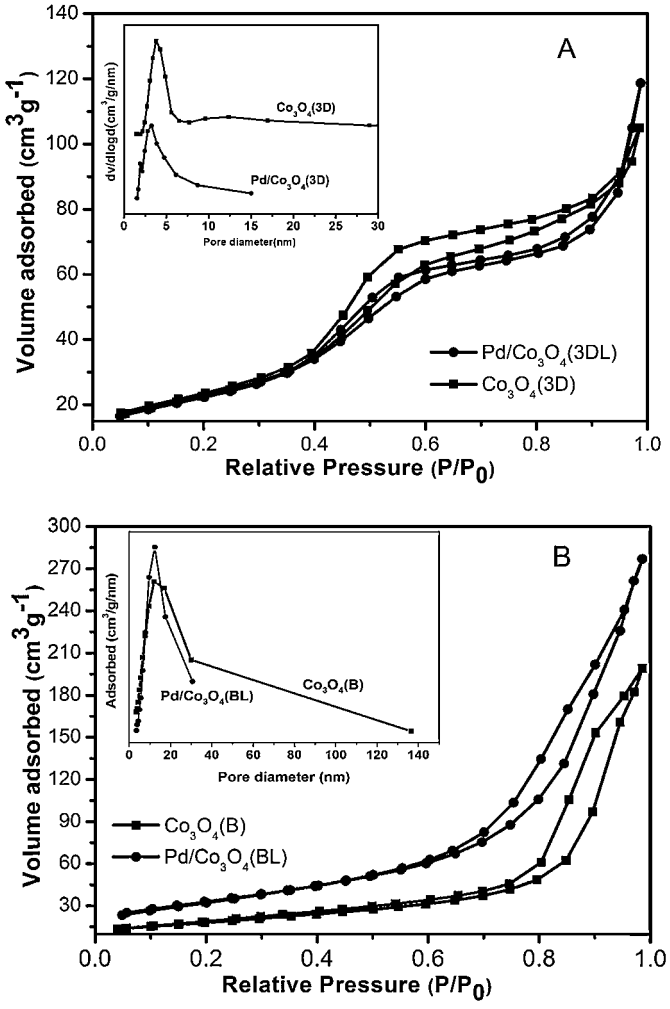


**Fig. 4.** $N_2$ adsorption–desorption isotherms and pore size distributions of the catalysts.

### 3.2.2. TEM

The catalysts were subjected to TEM measurements for their structure. Fig. 3 shows the TEM images of $Co_3O_4$ and $Pd/Co_3O_4$ catalysts. As shown in Fig. 3(a), the ordered mesoporous structure was clearly observed in $Co_3O_4$ (3D). After Pd loading, the mesopores were partially destroyed; however, the mesoporous structure still remained in the $Pd/Co_3O_4$ (3DL) catalysts (Fig. 3(b)). As shown in Fig. 3(c) and (d), the bulk $Co_3O_4$ (B) and $Pd/Co_3O_4$ (BL) did not show any ordered mesoporous structures. No obvious PdO species can be directly observed in the TEM images. As shown in Fig. 3(e) and (f), HRTEM images of $Pd/Co_3O_4$ (3DL) and $Pd/Co_3O_4$ (BL) showed the 0.28 nm lattice spacing of $Co_3O_4$ (2 2 0) as well as the 0.46 nm (1 1 1) lattice spacing, and PdO was not observed by HRTEM.

### 3.2.3. BET

$N_2$ adsorption–desorption isotherms and pore size distributions (inset) of four catalysts are shown in Fig. 4. The sorption curves of both $Co_3O_4$ (3D) and $Pd/Co_3O_4$ (3DL) catalysts (in Fig. 3a) exhibited slightly distorted Type-IV isotherms in the relative pressure range of 0.4–0.8, reconfirming the formation of a mesoporous structure [15]. The capillary condensation steps of the $Co_3O_4$ (3D) and $Pd/Co_3O_4$ (3DL) are not pronounced, indicating the relatively small sizes of ordered domains [11]. From the data of pore size distributions (inset in Fig. 4A), it can be seen that there were peaks at 4.8 and 3.4 nm observed over $Co_3O_4$ (3D) and $Pd/Co_3O_4$ (3DL), respectively. The mesoporous $Co_3O_4$ (3D) and $Pd/Co_3O_4$ (3DL) both have

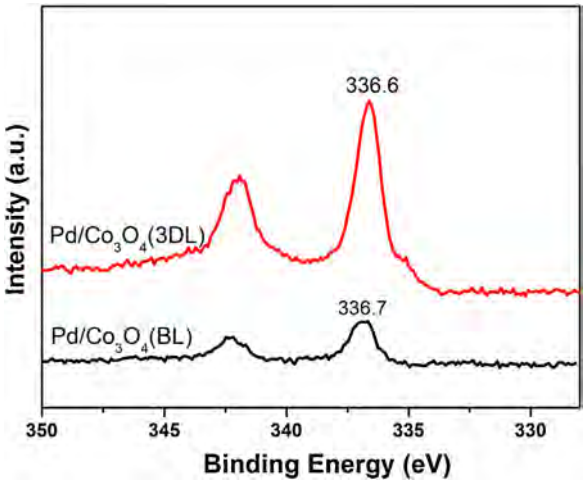


**Fig. 5.** Pd 3d XPS spectra of $Pd/Co_3O_4$ (3DL) and $Pd/Co_3O_4$ (BL).

a narrow distribution of pore size. Compared with the mesoporous catalysts, both $Co_3O_4$ (B) and $Pd/Co_3O_4$ (BL) exhibited Type H3 loops (Fig. 4B), which indicates the aggregation of $Co_3O_4$ particles, giving rise to slit-shaped pores [15].

The textural properties of these catalysts were shown in Table S2. The surface area of $Co_3O_4$ (3D) was 82 $m^2/g$. After Pd loading, the surface area of $Pd/Co_3O_4$ (3DL) decreased to 65 $m^2/g$, possibly because the mesostructure was partial destroyed by Pd introduction. In addition, the $Co_3O_4$ (B) and $Pd/Co_3O_4$ (BL) catalysts showed higher surface area than the mesoporous catalysts, presenting the surface area of 98 and 108 $m^2/g$, respectively. It is interesting to note that the surface area of $Pd/Co_3O_4$ (3DL) decreased with the average pore diameter decreased, but that is the opposite for $Pd/Co_3O_4$ (BL). The observed difference in surface area due to that surface energy for $Co_3O_4$ is due to changes in the bulk structure, such as variations in $Co^{3+}$ distribution in the defect spinel structure [27]. The surface area is not the main factor which affects the catalytic activity of these catalysts.

According to XRD, TEM and BET characterization, the results showed that the $Co_3O_4$ (3D) and $Pd/Co_3O_4$ (3DL) catalysts had the 3D-ordered mesoporous structure. Compared to bulk samples, the presence of the 3D-ordered mesoporous structure is favorable for the diffusion of the reactant molecules to the active sites [18,19]. Therefore, the ordered mesoporous structure was more beneficial for o-xylene oxidation.

### 3.3. Surface analysis—XPS

The XPS analysis was performed to verify the state and atomic concentration of Pd on the surface. As shown in Fig. 5, the Pd 3d XPS spectra clearly indicated that Pd was present as the oxide ($BE_{(Pd5/2)}$ higher than 335.6 eV) on both catalysts [23]. From the XPS spectra (Fig. 6), the atomic concentration of Pd, Co, O and Pd/Co atomic ratios are calculated and shown in Table 1. Based on the amount of Co, it is obvious that $Pd/Co_3O_4$ (3DL) presented much greater Pd/Co atomic ratio (5.60%) than that (0.58%) of $Pd/Co_3O_4$ (BL), suggesting

**Table 1**
XPS results for $Pd/Co_3O_4$ (3DL) and $Pd/Co_3O_4$ (BL): atomic concentration of Pd, Co, and O; the atomic ratio of Pd/Co.

| Catalyst | Atomic concentration (%) | | | Pd/Co (%) | Pd particle size (nm) |
|---|---|---|---|---|---|
| | Pd | O | Co | | |
| $Pd/Co_3O_4$ (3DL) | 1.69 | 68.37 | 29.94 | 5.60 | 8.2 [20] |
| $Pd/Co_3O_4$ (BL) | 0.19 | 67.51 | 32.30 | 0.58 | – |

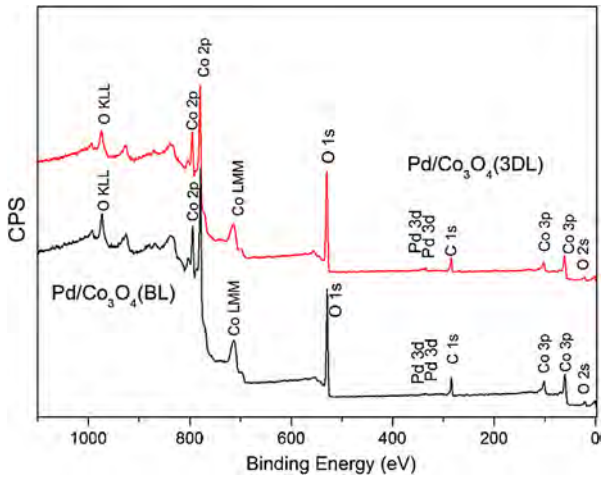


**Fig. 6.** The XPS spectra of $Pd/Co_3O_4$ (3DL) and $Pd/Co_3O_4$ (BL).

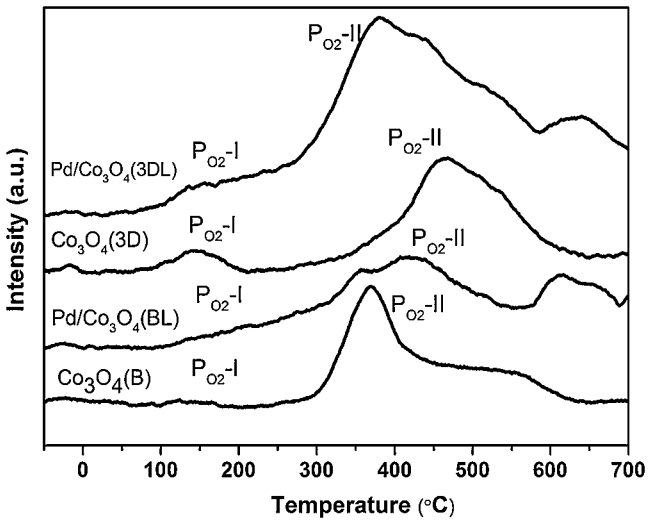


**Fig. 8.** $O_2$-TPD of $Co_3O_4$ and $Pd/Co_3O_4$ catalysts.

that PdO is more exposed on the surface of $Co_3O_4$ (3D). For its open mesoporous structure, the surface includes both inner and outer surfaces of the mesopores in surface layers of $Pd/Co_3O_4$ (3DL). The obvious difference of the Pd/Co atomic ratios was related to the different structure of the catalysts. It seems that most of PdO species were exposed on the surface of pore wall of the mesostructure without embedding, because the particle size (8.2 nm) of Pd species was larger than the thickness (6.3 nm) of the pore wall and its structure is an open 3D mesostructure [20]. For the $Pd/Co_3O_4$ (BL) catalyst, PdO species might be embedded in the pores accumulated by the bulk $Co_3O_4$ (B) particles, resulting in the weaker XPS peak intensity.

### 3.4. Chemical characteristic

#### 3.4.1. $H_2$-TPR

With different structure and exposed active site, the catalysts exhibited different catalytic performance because of the different chemical characteristic.

To investigate the reducibility of the samples, the $H_2$-TPR profiles of the catalysts were measured. Fig. 7 shows the $H_2$-TPR profiles of the catalysts. The $Co_3O_4$ (3D) sample shows three reduction peaks at 190, 320 and 430 °C assigned to the surface oxygen ($Peak_I$), $Co^{3+} \rightarrow Co^{2+}$($Peak_{II}$) and $Co^{2+} \rightarrow Co^0$ ($Peak_{III}$) reductions, respectively [22,24]. A sharp reduction peak ($Peak_0$) at 164 °C due to the PdO reduction and $Peak_I$ were observed on the $Pd/Co_3O_4$ (3DL) sample. $Peak_{II}$ and $Peak_{III}$ of $Pd/Co_3O_4$ (3DL) were both shifted to lower temperature, indicating that the introduction of PdO facilitated the reduction of $Co_3O_4$ (3D) due to the $H_2$ spillover effect. $Peak_{II}$ and $Peak_{III}$ appeared at 275 and 365 °C on $Co_3O_4$ (B), and were shifted to 260 and 344 °C on $Pd/Co_3O_4$ (BL) by $H_2$. As shown in Fig. 7, the reduction peak intensity of $Peak_{II}$ for $Pd/Co_3O_4$ (3D) and $Pd/Co_3O_4$ (BL) is larger than the intensity for $Co_3O_4$ (3D) and $Co_3O_4$ (B). The difference results from the interaction between Pd and $Co_3O_4$. When PdO was reduced to $Pd^0$, adjacent cobalt oxides were reduced to $Co^0$ in a single step ($Peak_{II}$) due to the $H_2$ spillover. The same phenomenon was also found in the literature [28]. It is obvious that after Pd addition the reducibility of $Pd/Co_3O_4$ (3DL) is enhanced much larger than that of $Pd/Co_3O_4$ (BL) catalyst due to the strong interaction between PdO and the $Co_3O_4$ (3D) support. A wide $Peak_0$ (PdO reduction) was observed at 225 °C on $Pd/Co_3O_4$ (BL), which is a much higher temperature than that (164 °C) on $Pd/Co_3O_4$ (3DL). But it is clearly seen that the $Peak_0$ of $Pd/Co_3O_4$ (3DL) is separate and occurs at low temperature, compared to the peak of $Pd/Co_3O_4$ (BL), indicating that PdO on $Co_3O_4$ (3D) had a better redox property than that on $Co_3O_4$ (B) because of the lower temperature for Pd reduction. For the $Pd/Co_3O_4$ (BL) catalyst, the reduction peaks of PdO and $Co_3O_4$ ($Peak_0$ and $Peak_{II}$) were overlapped, which was not the same as the separate reduction peak of PdO ($Peak_0$) of $Pd/Co_3O_4$ (3DL). These results suggested that PdO is more exposed on the surface of $Co_3O_4$ (3D) than that of $Co_3O_4$ (B), which agreed with the XPS result that Pd species seemed embedded on $Pd/Co_3O_4$ (BL). The XPS and TPR results reveal that the mesostructure would provide more exposed PdO species on the surface, which could improve the catalytic performance of the catalysts for o-xylene conversion.

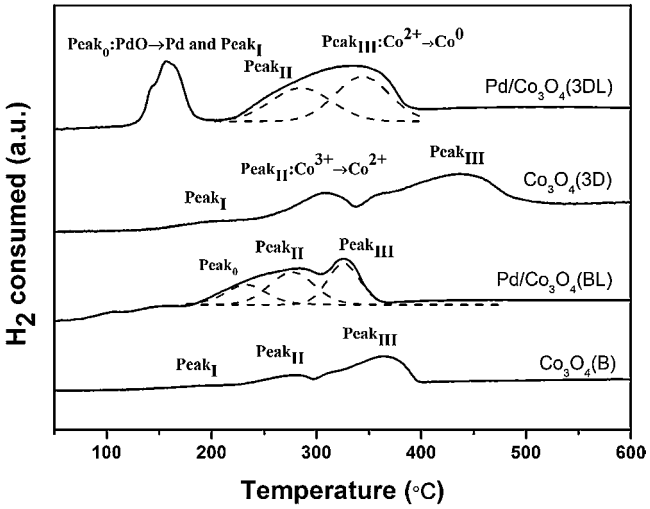


**Fig. 7.** $H_2$-TPR profiles of the catalysts.

#### 3.4.2. $O_2$-TPD

To clarify whether there is a relationship between the activity and the desorbed oxygen species on the catalyst, $O_2$-TPD experiments were performed over the catalysts. Fig. 8 shows $O_2$-TPD profiles of fresh catalysts. The $P_{O_2}$-I peak obtained at 100–300 °C is ascribed to the desorption of surface oxygen species such as $O^{2-}$ and $O^-$, and the $P_{O_2}$-II peak above 300 °C is attributed to the desorption of lattice oxygen in $Co_3O_4$ [22]. Compared to $Co_3O_4$ (B) and $Pd/Co_3O_4$ (BL), a clear $P_{O_2}$-I peak was observed on $Co_3O_4$ (3D) and $Pd/Co_3O_4$ (3DL), indicating that the mesoporous samples have more surface oxygen species. In addition, both $Co_3O_4$ (3D) and $Co_3O_4$ (B) presented $P_{O_2}$-II peaks, and the $P_{O_2}$-II peaks were

**Table 2**
The amount of oxygen species desorbed in $P_{O_2}$-I and $P_{O_2}$-II.

| $Peak_{O2}$-x | $Pd/Co_3O_4$ (3DL) | $Co_3O_4$ (3D) | $Pd/Co_3O_4$ (BL) | $Co_3O_4$ (B) |
|---|---|---|---|---|
| $P_{O_2}$-I (μmol/g cat)[a] | 290 | 150 | 140 | 29 |
| $P_{O_2}$-II (μmol/g cat)[a] | 662 | 468 | 626 | 420 |

[a]The amount of oxygen species was calculated from $P_{O_2}$-I and $P_{O_2}$-II of each profile in Fig. 5.

clearly strengthened after Pd loading because PdO activated the lattice oxygen [25,26]. For better comparison, the amounts of $O_2$ desorbed in $P_{O_2}$-I and $P_{O_2}$-II (integration area) are listed in Table 2. As shown in Table 2, $Co_3O_4$ (3D) has much larger $P_{O_2}$-I and $P_{O_2}$-II peak areas than $Co_3O_4$ (B), and $Pd/Co_3O_4$ (3DL) has the largest peak area among the four catalysts, indicating that the mesoporous samples have more surface oxygen species for the o-xylene oxidation in the low temperature range. The reaction occurred in the temperature range from 100 to 300 °C over $Co_3O_4$ (3D) and $Co_3O_4$ (B), and the surface oxygen species of $Co_3O_4$ (3D) were much more than that of $Co_3O_4$ (B), indicating that the better catalytic activity of $Co_3O_4$ (3D) was attributed to more surface oxygen species. The more surface oxygen species was also confirmed by XPS measurement. As shown in the Co 2p XPS data (Fig. S1), $Co_3O_4$ (3D) exhibited higher molar ratio of $Co^{2+}/Co^{3+}$ and $O_{Surface}/O_{Lattice}$ than $Co_3O_4$ (B), which indicated higher surface oxygen vacancy density on the surface of $Co_3O_4$ (3D), resulting in more surface oxygen species activated. This result confirms the facile activation of oxygen molecules on $Co_3O_4$ (3D). After Pd loading, the catalysts showed better activity than the supports (Fig. 1) and an interaction between Pd and $Co_3O_4$ was responsible for their activity enhancement. It is obvious that the two desorbed oxygen peaks ($P_{O_2}$-I and $P_{O_2}$-II) were overlapped, indicating that the lattice oxygen of cobalt oxides was clearly activated by Pd and the activated oxygen atoms are rather mobile and reactive, readily reacting with the adsorbed o-xylene through spillover [29]. Therefore, both surface oxygen and activated lattice oxygen plays an important role in the o-xylene oxidation reaction over $Pd/Co_3O_4$ (BL) and $Pd/Co_3O_4$ (3DL).

Based on these findings, we can reveal that the mesoporous structure could provide more exposed PdO species and more surface oxygen species. In addition, a stronger interaction between Pd and $Co_3O_4$ would offer more activated lattice oxygen species. The mesostructure and interaction had an important influence on the catalytic activity for o-xylene oxidation.

## 4. Conclusions

Compared with $Co_3O_4$ (B), mesoporous $Co_3O_4$ (3D) exhibited higher activity for catalytic oxidation of o-xylene. The loading of Pd shows slight effect on the original mesoporous structure of $Co_3O_4$ (3D), and Pd addition greatly enhanced its catalytic performance. The $Pd/Co_3O_4$ (3DL) catalyst showed the highest activity for o-xylene oxidation among the four catalysts and it presented 90% o-xylene conversion at 249 °C. The excellent catalytic performance of $Pd/Co_3O_4$ (3DL) might be due to the mesoporous structure, the more exposed PdO species on $Co_3O_4$ (3D) and the high activity of oxygen species. The surface oxygen and activated lattice oxygen of cobalt oxides would be responsible for their activity in o-xylene oxidation.

## Acknowledgments

This work was financially supported by the National Natural Science Foundation for Creative Research Groups of China (51221892) and the National High Technology Research and Development Program of China (2012AA062702).

## Appendix A. Supplementary data

Supplementary data associated with this article can be found, in the online version, at http://dx.doi.org/10.1016/j.cattod.2014.06.032.

## References

[1] A. Jones, Atmos. Environ. 33 (1999) 4535–4564.
[2] J.J. Spivey, Ind. Eng. Chem. Res. 26 (1987) 2165–2180.
[3] F.I. Khan, A. Kr Ghoshal, J. Loss Prevent. Proc. 13 (2000) 527–545.
[4] J.N. Armor, Appl. Catal. B 1 (1992) 221–256.
[5] L.F. Liotta, Appl. Catal. B 100 (2010) 403–412.
[6] S.C. Kim, W.G. Shim, Appl. Catal. B 92 (2009) 429–436.
[7] G. Centi, J. Mol. Catal. A Chem. 173 (2001) 287–312.
[8] P. Yang, D. Zhao, D.I. Margolese, B.F. Chmelka2, G.D. Stucky, Nature 396 (1998) 152–155.
[9] B. Lee, D. Lu, J.N. Kondo, K. Domen, Chem. Commun. (2001) 2118–2119.
[10] F. Jiao, P.G. Bruce, Adv. Mater. 19 (2007) 657–660.
[11] A. Rumplecker, F. Kleitz, E.L. Salabas, F. Schüth, Chem. Mater. 19 (2007) 485–496.
[12] A.K. Sinha, K. Suzuki, Appl. Catal. B 70 (2007) 417–422.
[13] H. Tüysüz, M. Comotti, F. Schüth, Chem. Commun. (2008) 4022–4024.
[14] A. Sayari, P. Liu, Micropor. Mater. 12 (1997) 149–177.
[15] M. Kruk, M. Jaroniec, Chem. Mater. 13 (2001) 3169–3183.
[16] B. Tian, X. Liu, L.A. Solovyov, Z. Liu, H. Yang, Z. Zhang, S. Xie, F. Zhang, B. Tu, C. Yu, J. Am. Chem. Soc. 126 (2004) 865–875.
[17] T. Tsoncheva, L. Ivanova, J. Rosenholm, M. Linden, Appl. Catal. B 89 (2009) 365–374.
[18] Y. Xia, H. Dai, H. Jiang, L. Zhang, Catal. Commun. 11 (2010) 1171–1175.
[19] J. Deng, L. Zhang, H. Dai, Y. Xia, H. Jiang, H. Zhang, H. He, J. Phys. Chem. C 114 (2010) 2694–2700.
[20] Y. Wang, C. Zhang, F. Liu, H. He, Appl. Catal. B: Environ. 142–143 (2013) 72–79.
[21] Y. Yu, T. Takei, H. Ohashi, H. He, X. Zhang, M. Haruta, J. Catal. 267 (2009) 121–128.
[22] L. Xue, H. He, C. Liu, C. Zhang, B. Zhang, Environ. Sci. Technol. 43 (2009) 890–895.
[23] G.E. Muilenberg, Handbook of X-Ray Photoelectron Spectroscopy, Perkin-Elmer, Minnesota, 1979.
[24] T. Tsoncheva, L. Ivanova, J. Rosenholm, M. Linden, Appl. Catal. B: Environ. 89 (2009) 365–374.
[25] K. Yamamuro, S. Tamura, R. Watanabe, Y. Sekine, Catal. Lett. 143 (2013) 339–344.
[26] J. Lojewska, A. Kolodziej, J. Zak, J. Stoch, Catal. Today 105 (2005) 655–661.
[27] J.M. McHale, A. Navrotsky, A.J. Perrotta, J. Phys. Chem. B 101 (1997) 603–613.
[28] N. Acerbi, S.C. Tsang, G. Jones, S. Golunski, P. Collier, Angew. Chem. Int. Ed. 52 (2013) 7737–7741.
[29] J.Y. Luo, et al., J. Catal. 254 (2008) 310–324.